Available online at www.sciencedirect.com
ScienceDirect
Acta Materialia 59 (2011) 6287–6296
Acta MATERIALIA
www.elsevier.com/locate/actamat

Spectral evidence of spinodal decomposition, phase transformation and molecular nitrogen formation in supersaturated TiAlN films upon annealing

J.L. Endrino [a,*], C. Århammar [b], A. Gutiérrez [c], R. Gago [a], D. Horwat [d], L. Soriano [c], G. Fox-Rabinovich [e], D. Martín y Marero [c,f,g], J. Guo [h], J.-E. Rubensson [i], J. Andersson [j]

[a] Instituto de Ciencia de Materiales de Madrid, Consejo Superior de Investigaciones Científicas, E-28049 Madrid, Spain
[b] Sandvik Tooling AB, R&D, Lerkrogsvägen 13, 126 80 Stockholm, Sweden
[c] Departamento de Física Aplicada and Instituto de Ciencia de Materiales Nicolás Cabrera, Universidad Autónoma de Madrid, E-28049 Madrid, Spain
[d] Institut Jean Lamour, Ecole des Mines de Nancy, Parc de Saurupt, 54042 Nancy, France
[e] McMaster University, Hamilton, Ontario, Canada L8S 4L7
[f] Fundación Parque Científico de Madrid, Campus de Cantoblanco, 28049 Madrid, Spain
[g] Centro de Microanálisis de Materiales, Universidad Autónoma de Madrid, 28049 Madrid, Spain
[h] Advanced Light Source, Lawrence Berkeley National Laboratory, 1 Cyclotron Rd., Berkeley, CA 94720, USA
[i] Department of Physics and Astronomy, Uppsala University, Box 516, S-75120 Uppsala, Sweden
[j] The Angstrom Laboratory, Uppsala University, S-75121 Uppsala, Sweden

Received 4 December 2010; received in revised form 22 June 2011; accepted 22 June 2011
Available online 21 July 2011

Abstract

Thermal treatment of supersaturated $Ti_{1-x}Al_xN$ films ($x \approx 0.67$) with a dominant ternary cubic-phase were performed in the 700–1000 °C range. Grazing incidence X-ray diffraction (GIXRD) shows that, for annealing temperatures up to 800 °C, the film structure undergoes the formation of coherent cubic AlN (c-AlN) and TiN (c-TiN) nanocrystallites via spinodal decomposition and, at higher temperatures ($\geqslant$900 °C), GIXRD shows that the c-AlN phase transforms into the thermodynamically more stable hexagonal AlN (h-AlN). X-ray absorption near-edge structure (XANES) at the Ti *K*-edge is consistent with spinodal decomposition taking place at 800 °C, while Al *K*-edge and N *K*-edge XANES and X-ray emission data show the nucleation of the h-AlN phase at temperatures >800 °C, in agreement with the two-step decomposition process for rock-salt structured TiAlN, which was also supported by X-ray diffraction patterns and first-principle calculations. Further, the resonant inelastic X-ray scattering technique near the N *K*-edge revealed that N_2 is formed as a consequence of the phase transformation process.

Keywords: TiAlN; Nanocrystalline materials; X-ray absorption near-edge structure; Resonant inelastic X-ray scattering

1. Introduction

The development of hard and wear-resistant thin film nanomaterials for specific applications has been the objective of numerous investigations in recent years [1,2]. The focus has been primarily on the design of new thin film compositions with improved physical properties at the temperature of application. New methods such as resonant inelastic X-ray scattering (RIXS) have become available for characterizing the bonding and electronic structure of materials [3]. Such methods can be used to characterize new complex nanostructured thin films and to attain better fundamental knowledge of these key materials.

Al-rich $Ti_{1-x}Al_xN$ coatings are widely used for high temperature, high wear resistance applications, and it is

* Corresponding author.
E-mail address: jlendrino@icmm.csic.es (J.L. Endrino).

1359-6454/$36.00 © 2011 Acta Materialia Inc. Published by Elsevier Ltd. All rights reserved.
doi:10.1016/j.actamat.2011.06.039

known that annealing of $Ti_{1-x}Al_xN$ coatings can result in hardness improvements at elevated temperatures [4–7]. The most common explanation for this phenomenon is the generation of a high micro-stress level at the c-AlN/c-AlTiN interfaces, which leads to an increase in microhardness. This is the opposite trend to that which occurs in standard titanium nitride films deposited at intermediate temperatures, where annealing can lead to significant stress relief [8]. However, with regard to dealing with Al-rich $Ti_{1-x}Al_xN$, not all coatings are alike, even those with identical chemical compositions. Slight process parameter variations employed in the deposition recipes result in coatings with significant differences in mechanical properties and wear performance [9]. This has been one of the topical issues engaging coating designers in recent years. The nanocrystalline structure and near-amorphous nature of certain Al-rich $Ti_{1-x}Al_xN$ compositions ($0.6 < x < 0.7$) make it a complex task for coating developers to differentiate between some of the key structural features using conventional laboratory techniques. Owing to the high amount of aluminum, the Al–Ti–N coating has a very fine-grained nanocrystalline structure (grain size ~5 nm). The specifics of the interatomic bonds in the crystal lattice of $Ti_{1-x}Al_xN$ affect their physical properties such as plasticity and hardness. The electronic structure indicates formation of metallic bonds, resulting in an increase in plasticity at the cost of hot hardness reduction. The surface is then able to dissipate energy by means of plastic deformation (instead of crack formation) and, in this way, surface damage might be reduced. Addition of aluminum can significantly increase the energy band gap between the conduction band (CB) and the valence band (VB), reducing the metallic character of the interatomic bonds in the $Ti_{1-x}Al_xN$ lattice and, as a consequence, this material obtains properties closer to that of a semiconductor [10].

Recently, owing to its elemental and local character selectivity, synchrotron radiation techniques such as X-ray absorption near-edge structure (XANES) have been successfully employed to resolve the bonding structure of $Ti_{1-x}Al_xN$ coatings and to monitor the Al incorporation into the cubic cell [11,12]. In addition, XANES has been used to point out the formation of Ti–Al bonds as a result of the segregation of the wurtzite phase [11]. Moreover, the solubility of silicon in ternary and quaternary nitrides, depending on their crystalline structure was recently reported [13].

Although the decomposition of metastable $Ti_{1-x}Al_xN$ with NaCl-type structure (c-$Ti_{1-x}Al_xN$) upon annealing has been the subject of considerable research effort in the last decade [6,10,14], the structural evolution of borderline supersaturated (where there are mixed hexagonal and cubic phases) $Ti_{1-x}Al_xN$ films with annealing temperature is still unknown. Phase separation of c-$Ti_{1-x}Al_xN$ into coherent cubic domains has been explained by spinodal decomposition of the metastable ternary solid solution upon annealing [5,6,14–17]. According to a recent theoretical investigation, the mixing enthalpy of cubic TiN (c-TiN) and AlN (c-AlN) phases is very high, primarily due to the unfavorable localization of Ti non-bonding electronic states [10]. The high mixing enthalpy leads to the possibility of a negative second derivative of the free energy with respect to composition and, therefore, also the prospect of spinodal decomposition.

In a study by Hörling et al. [5], the asymmetric broadening of X-ray diffraction (XRD) peaks from the cubic phase in coatings of $Ti_{0.34}Al_{0.66}N$ annealed at 900 °C were interpreted as spinodal decomposition. More recently, compositional segregations of Ti and Al in $Ti_{0.34}Al_{0.66}N$/TiN multilayer coatings annealed at 900 °C were revealed by scanning transmission electron microscopy (STEM) elemental mapping [15]. High-resolution TEM showed Al-rich coherent domains that were consistent with a spinodal-type decomposition of $Ti_{1-x}Al_xN$ into c-TiN and c-AlN. However, definite evidence of such spinodal decomposition is still desirable.

It has also been reported that the Al content and distribution, together with structural disorder, can play a significant role in the compound evolution and stability upon annealing [6]. In a supersaturated state it is possible that the Al distribution can lead to small segregations of the hexagonal AlN (h-AlN) phase. Hugosson et al. [18] reported that alloying transition metal carbides with competing structures can create polytypic compounds in which the propagation of dislocations can be strongly suppressed by a large number of interfaces between structures with different glide systems. This concept can also be extended to the $Ti_{1-x}Al_xN$ system in order to optimize the mechanical performance in a specific application. For some applications, it was shown that only a very small amount of such h-AlN phase could be tolerated, owing to the concomitant reduction in hardness [4,19]. However, even though this phase formation reduces hardness, it also refines grain size and improves ductility, which is of critical importance for some unstable wear modes such as attrition wear, which is typical for machining of widely used hard-to-cut aerospace alloys (titanium alloys and nickel-based superalloys) [4], for instance, as well as for machining of austenitic stainless steels [9] among many other technological applications. This study reports on the evolution of such a supersaturated $Ti_{1-x}Al_xN$ system, using a variety of advanced synchrotron radiation spectroscopic techniques. Using the spectroscopic fingerprints of supersaturated $Ti_{1-x}Al_xN$ films annealed up to 1000 °C in correlation with XRD analysis, the spinodal decomposition of the cubic ternary $Ti_{1-x}Al_xN$ phase, the subsequent transformation of c-AlN domains to h-AlN and the formation of a fraction of molecular nitrogen are confirmed.

2. Experimental details

The Al-rich $Ti_{1-x}Al_xN$ hard coatings were synthesized using Oerlikon Balzers' Rapid Coating System deposition equipment in a cathodic arc ion-plating mode using $Al_{67}Ti_{33}$ targets. The system also incorporated two pure Ti targets to synthesize a pure metallic adhesion layer

(~30 nm thick). Prior to deposition, the substrates, mirror polished cemented carbide WC/Co turning inserts, were heated and plasma etched using an argon ion etching process. For the deposition of the $Ti_{1-x}Al_xN$ layer, the chamber was back-filled with a pure reactive nitrogen atmosphere, and the pressure was in the range 0.1–3 Pa. The substrates had threefold rotation, and they were heated to a temperature of ~600 °C prior to deposition. In order to control the substrate temperature, thermocouples were placed in the fixed part of the rotating carousel and in the line of sight of the substrates. These thermocouples are needed in order to control the irradiative heaters placed in two levels in the chamber walls before deposition. During the deposition, an average bias voltage of −100 V was also applied to the substrates. The average distance from the cathode was 35 cm, and the deposition times were adjusted in order to achieve coating thicknesses of 3.5 ± 0.2 μm. The annealing experiments on the coated samples were performed in high vacuum at 1×10^{-6} mbar for 2 h. The samples, annealed at temperatures of 800 °C or lower, kept the same light blue–gray appearance, while the samples annealed at higher temperatures showed a slight color change towards dark gray, probably due to a small amount of surface tarnishing.

The chemical composition was determined by Rutherford backscattering spectrometry (RBS) with a 5-MV HVEE Tandetron accelerator sited at the Centro de Micro-Análisis de Materiales at Universidad Autónoma de Madrid. RBS spectra were collected using a 2-MeV He^+ beam. In order to improve the sensitivity to nitrogen, experiments at 3.71 MeV were also collected in order to have [14] N(α, α) resonance. The composition of the samples is shown in Table 1; all the compositional data are within ±1 at.% error. The structural characteristics of the films were probed by grazing incidence X-ray diffraction (GIXRD) at an incident angle of 2° with respect to the substrate surface. The experiments were done with a Co K_α source (wavelength 0.179 nm) using an INEL diffractometer. The lattice parameters and respective errors were determined from single peak analysis of (1 0 0) for w-$Ti_{1-x}Al_xN$ and (2 0 0) for c-$Ti_{1-x}Al_xN$.

Total energy and electronic structure calculations were performed using density functional theory and the projector augmented wave method [20] as implemented in the Vienna Ab Initio Simulation Package [21]. The generalized gradient approximation Perdew–Burke–Ernzerhof functional was used [22,23]. The atomic geometries were fully optimized until the Hellmann–Feynmann forces on each atom were less than the threshold value of 10^{-5} eV Å^{-1}. To ensure convergence of energy, a cutoff of 800 eV was used for the plane wave expansion of the wave function and a $8 \times 8 \times 8$ k-points mesh for all investigated systems. A full structure relaxation (volume, atom positions and shape of the cell) was performed in all calculations. Primitive cells were used to model c-TiN and h-AlN. A $2 \times 2 \times 1$ supercell consisting of 32 atoms was used for modeling c-$Ti_{1-x}Al_xN$. Of these 32 atoms, 16 were on the cation lattice and 16 on the anion lattice. The Al atoms were distributed onto the cation lattice, such that four different coordinations of N–Me_6, where Me = Al, Ti, were considered.

Table 1
RBS chemical composition analysis using 3.710 MeV He^+ for as-deposited and annealed Ti–Al–N.

Sample	N (at.%)	Al (at.%)	Ti (at.%)
As-deposited	51	32	17
700 °C	51	32	17
800 °C	51	31	18
900 °C	51	31	18
1000 °C	52	31	17

The bonding structure of the films with elemental sensitivity to local environments of N, Ti and Al sites was studied by XANES. Measurements with soft (N 1s and Al 1s edges at 400 and 1800 eV) and hard (Ti 1s between 4950 and 5100 eV) X-rays were carried out at the Canadian Light Source (CLS) synchrotron using the SGM beamline and at BESSY-II (Berlin, Germany) synchrotron facility using the KMC-2 beamline, respectively. Soft X-ray measurements were performed in both total electron yield and total fluorescence yield (TFY) modes, while hard X-ray measurements were performed only in TFY mode. The spectra reported in the figures of this article were collected in TFY mode and, consequently, the analysis and conclusions drawn correspond to changes only within the bulk of the $Ti_{1-x}Al_xN$ layer and not to superficial effects, which could be influenced by the slight surface tarnishing or by the presence of surface macroparticles. Both emission and RIXS spectra were recorded at the Advanced Light Source (Berkeley, CA) using beamline 7.0.1 incorporating a Nordgren-type grazing-incidence spherical grating spectrometer [24] with the energy resolution set to 0.4 eV at the N K-edge. The incident photon energy was calibrated to a hexagonal BN reference sample, measured during the experiments. The energy resolution of the incoming photons was set to 0.4 eV for the emission spectra measurements. The emission energies were calibrated to the elastic features of emission spectra of the N K-edge of the BN reference sample.

3. Results and discussion

3.1. Structural analysis by GIXRD

Fig. 1a shows the GIXRD patterns for the film as deposited and annealed at 700, 800, 900 and 1000 °C. The diffractograms clearly exhibit the signature of the cubic c-$Ti_{1-x}Al_xN$ ternary phase with diffraction lines between those of c-TiN and c-AlN. Reflections in the vicinity of the theoretical positions of the h-AlN phase are also observed for all the conditions. The evolution of the cell parameter for the cubic (a_C) and hexagonal/wurzite (a_W) phases is plotted in Fig. 1b and c, respectively.

The size of the cubic cell remains nearly unchanged between room temperature and 800 °C before sharply

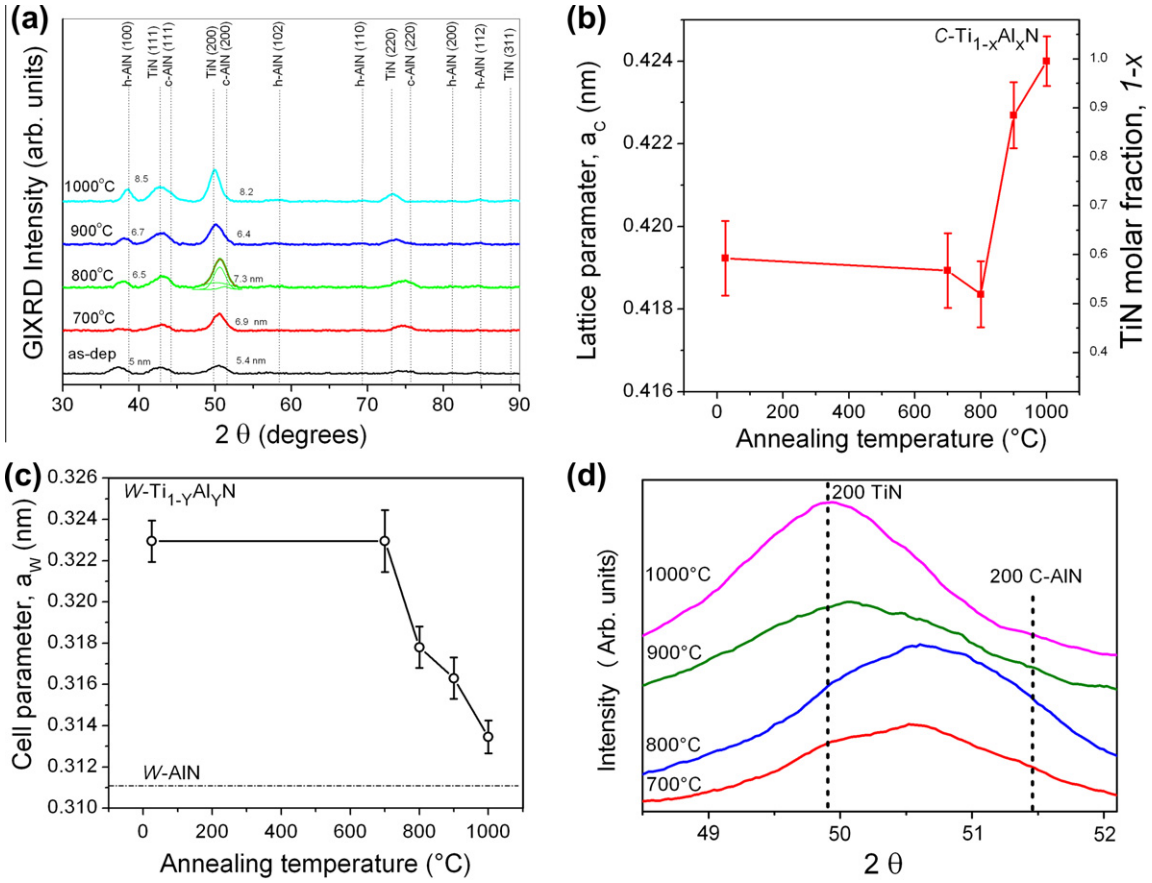

Fig. 1. (a) XRD patterns for $Ti_{33}Al_{67}N$ in as-deposited (as-dep) state and after annealing in vacuum at various temperatures. (b) Lattice parameter (a_C) of face-centered cubic $Ti_{1-x}Al_xN$ and estimated TiN molar fraction. (c) Cell parameter (a_W) of hexagonal close-packed $Ti_{1-y}Al_yN$. (d) Magnified view of the 200 diffraction peaks of the annealed films.

rising up to that of TiN. In contrast, a_W starts to shrink at 700 °C and approaches the value of w-AlN at 1000 °C. In parallel, the c_W/a_W cell parameters ratio is stable at 1.6, indicating a homogeneous deformation of the hexagonal lattice. Gago et al. [11] recently observed shrinkage of the c-$Ti_{1-x}Al_xN$ ternary solid solution upon Al incorporation. Thus, the expansion observed with heating can reasonably be ascribed to an increase in the atomic concentration of Ti in c-$Ti_{1-x}Al_xN$, as shown in Fig. 1b. The opposite geometrical variations observed for the two phases (Fig. 1b and c) suggest that titanium and aluminum atoms are exchanged at high temperature between the cubic and hexagonal regions of the films. Nevertheless, the onset temperature for cubic cell expansion is slightly higher than that of the wurtzite cell shrinkage. Fig. 1d shows magnified views of the ⟨2 0 0⟩ diffraction peaks of the annealed films. After the 700 °C treatment, the peak is asymmetric and presents a hump characteristic of TiN. The same is observed after the 800 °C treatment, but to a lower extent. This is in line with a separation of the original c-$Ti_{1-x}Al_xN$ in an Al-poor and an Al-rich phase upon heating in this temperature range, as usually reported for high Al content c-$Ti_{1-x}Al_xN$ thin films [4,6]. This may explain why the c-$Ti_{1-x}Al_xN$ expands after wurtzite shrinkage. At higher temperatures, the peak approaches the position of TiN and is symmetrical, even though a small contribution of ⟨2 0 0⟩ c-AlN can be hypothesized after a 1000 °C treatment.

In Fig. 2, the measured X-ray patterns at 800 °C and 1000 °C, along with patterns calculated from first principles, are displayed. The peak at 38.4° can be assigned to h-AlN, as can the peaks at 58.2° and 69.0°. The peaks at 50.6° and 74.3° are signatures of the c-$Ti_{1-x}Al_xN$ or c-TiN structure, whereas the peak at 43.4° could have a possible origin in h-AlN, c-TiN or c-$Ti_{1-x}Al_xN$ or in mixtures thereof. The broadening of this peak at 1000 °C compared with that at 800 °C might be caused by more significant h-AlN formation. Interesting to note is the small contribution from c-$Ti_{1-x}Al_xN$ at 58.2°, which is seen in the calculated X-ray pattern. This indicates that this peak would appear just by symmetry breaking in the c-$Ti_{1-x}Al_xN$ structure owing to the high Al-content. Moreover, the intensity ratio between the peak at 43.4° and 50.6° in the measured pattern is best matched by the calculated c-$Ti_{1-x}Al_xN$ pattern.

Finally, the grain size was calculated by the Scherrer formula [25] after subtraction of the peak broadening from the

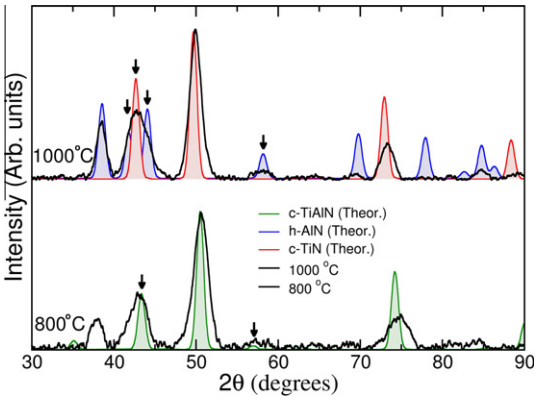

Fig. 2. X-ray diffractogram for $Ti_{33}Al_{67}N$ after annealing in vacuum at 800 and 1000 °C along with the calculated X-ray patterns of c-TiAlN (supercell model), h-AlN and c-TiN. The calculated patterns have been matched to the height of the peak with maximum peak area in the experimental spectra (at 43.4° 2θ for h-AlN and at 50.6° 2θ for c-TiN and c-TiAlN).

experimental setup. The grain size average varied between 5 nm in the as-deposited state and 8.5 nm after the annealing process at 1000 °C, for both cubic and wurtzite phases.

3.2. X-ray absorption features

3.2.1. Ti(1s) edge

Fig. 3a presents the Ti 1s spectra of as-deposited and annealed $Ti_{33}Al_{67}N$ samples. The spectrum of a TiN sample (features A–C) is also shown here for comparison. For the as-deposited $Ti_{1-x}Al_xN$ sample, at low energy (<4975 eV), the spectrum shows a characteristic pre-edge peak (feature D), which is located at ~4967 eV. In a recent work on Ti *K*-edge of ternary Ti–Si–N films, the pre-edge peak of the Ti *K* spectra at this energy was assigned to Ti-d states hybridized with Si-p states [13]. Aluminum, like silicon, has p states at the CB; consequently, it is feasible to interpret that Ti-d states along with Al-p contribute to the pre-edge peak. However, this contribution should not be the only origin of the pre-edge peak: hybridization between Ti-d and N-p states is also possible, as evidenced in the TiN spectrum. In the annealed samples, feature D is shifted ~1.5 eV towards higher energy, and it is worth noting that the overall intensity of the pre-edge peak is decreased with annealing temperature, which is consistent with a decrease in the number of Ti–Al bonds and phase separation of c-$Ti_{1-x}Al_xN$ phase. Similarly, at the high energy region (>4980 eV), there is a sudden change at 800 °C in the lineshape of the Ti *K*-edge in $Ti_{1-x}Al_xN$ films, which is highlighted by the appearance of feature C at this temperature and the overall match of these spectra with that of the standard TiN sample (prepared using reactive cathodic arc deposition), which is additional evidence that some phase decomposition of the $Ti_{1-x}Al_xN$ phase has already taken place.

3.2.2. Al(1s) edge

Fig. 3b shows the Al(1s) edges of the as-deposited and annealed $Ti_{1-x}Al_xN$ samples, together with the spectrum from an h-AlN reference sample. The energy features (G–J) in the fine structure of the Al (1s) edge for h-AlN are related to transitions from Al (1s) to p and d hybridized orbitals [26]. Regarding the c-AlN allotrope, there is less information available, owing to its metastable character. As predicted theoretically [26], rock-salt AlN environments should present features distinct from those of h-AlN owing to the different coordination number. Experimentally, c-AlN fingerprints have been studied by stabilizing this phase

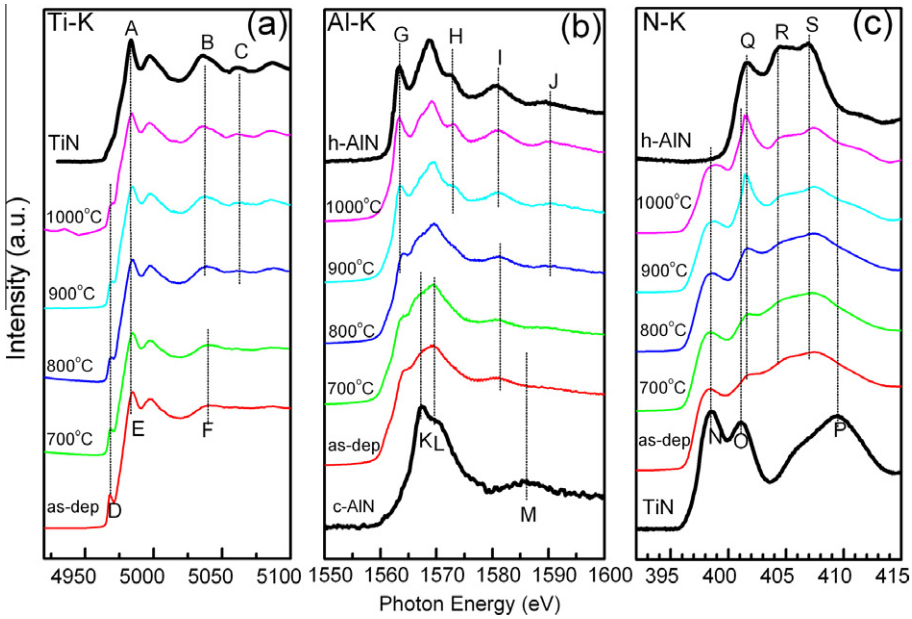

Fig. 3. (a) TFY X-ray absorption spectroscopy patterns for $Ti_{33}Al_{67}N$ in as-deposited (as-dep) state and after annealing in vacuum at various temperatures: (a) Ti *K*-edge; (b) Al *K*-edge; (c) N *K*-edge.

in short-period TiN/AlN multilayers under compressive stress [27] and upon segregation in low-carbon aluminum-killed steels [28]. In contrast to h-AlN, cubic arrangements should present a dominant single peak downshifted ~1 eV with respect to the main h-AlN feature (L). Similarly, feature (K), which is dominant in the c-AlN standard spectra (represented from theoretical prediction [26]), could also be correlated with the formation of cubic domains. Under these considerations, the maximum of intensity around feature L at the Al(1s) spectrum from the as-deposited films reveals that Al sites in this film are mainly cubic. The width of feature L in the as-deposited film is significantly larger than that reported for c-$Ti_{1-x}Al_xN$ ternary solutions grown by magnetron sputtering [11]. This fact could be attributed to a more disordered structure here, due to the effect of ion implantation damage caused by the high substrate bias and the high metal plasma density produced by the cathodic arc technique along with a high Al content which is close to that leading to nanocrystalline films [29]. A weak shoulder at the G position is also clear in the as-deposited film, indicating the reduced presence of h-AlN precipitates, in agreement with GIXRD. Clearly, on an increase in the annealing temperature, the intensity of features G, H, I and J are promoted owing to the increasing participation of h-AlN sites. The formation of h-AlN is significant > 900 °C.

3.2.3. N(1s) edge

The N 1s spectra (shown in Fig. 3c) of titanium nitride can be related to the density of unoccupied N-2p states with two clear regions related to hybridization with the empty Ti-d (397–404 eV) and Ti-4sp (404–414 eV) bands. The lineshape of the N 1s spectra in the h-AlN compound corresponds to unoccupied N-2p states hybridized with Al-3p states in the energy range 400–410 eV. The soft X-ray absorption (SXA) spectrum is polarization dependent and reflects the anisotropy of the unoccupied states in wurtzite AlN [30,31]. However, given the similar and random/disordered texture of the nanocrystalline h-AlN phase appearing in the films (as shown in Fig 1a), it is possible to compare between the samples. It is observed that there is some amount of overlap between the Ti-d and Al-p states which adds some complexity to the electronic structure analysis of nanocrystalline titanium aluminum nitrides. Indeed, the spectra of the as deposited $Ti_{33}Al_{67}N$ film show extensive filling of the edge with large broadened peaks in which it is difficult to separate both contributions. Specifically, feature O (in TiN) and feature Q (in AlN) are separated by ~0.5 eV; such a short distance is difficult to resolve, considering the large width of the $Ti_{33}Al_{67}N$ peaks. In addition, the $Ti_{33}Al_{67}N$ films annealed at temperatures >800 °C show the presence of a sharp feature at ~401.4 eV (which falls in between features O and Q), which will be discussed below.

In order to attain additional information, the c-TiN standard contribution normalized at ~398.5 eV has been subtracted from the N 1s TFY XANES for the various $Ti_{33}Al_{67}N$ samples and is shown in correlation to h-AlN and c-AlN spectral references in Fig. 4. It is observed that, after the subtraction, a shoulder peak at ~397.1 eV appears, and its intensity decreases with annealing temperature. The peak is associated with the large width of the peaks in the as-deposited sample compared with the highly crystalline c-TiN standard which was employed, and highlights the changes in the crystallinity of the sample upon annealing. Here, it is also observed that the N-2p empty states hybridized with Al-3p remain undisturbed until 800 °C. This is in good correlation with GIXRD data, since the constituent phases remain fundamentally cubic. At 900 °C and 1000 °C, a change in the overall lineshape is observed, which correlates well with the formation of the hexagonal phase. In addition, the existence of a sharp peak at ~401.4 eV is observed; the peak has fine structure which coincides with the vibrational fine structure of the π^* excited states of N_2. Although it would be difficult to quantify the overall mass of this feature with respect to the AlN phase (and consequently with respect to the entire film) owing to the close overlap with the first N 1s peak of the h-AlN spectrum (feature Q in Fig. 3c), this spectral feature could probably correspond to an amount of a "third phase" (possibly molecular N_2 trapped within the film), which could be formed during the phase transformation process as a residual substance. Owing to the slightly higher nitrogen content measured in the samples, it is reasonable to presume that, because of the deposition conditions, N is also incorporated into interstitial sites during the synthesis, causing some amount of microstrain, which

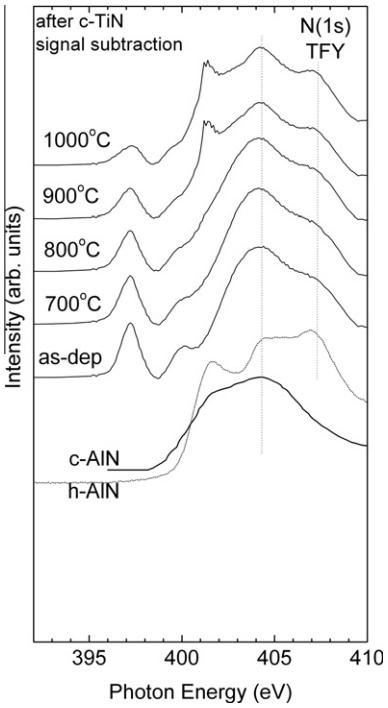

Fig. 4. N *K*-edge XAS patterns after c-TiN signal subtraction (normalized at 398 eV TiN standard peak) for as-deposited and annealed $Ti_{33}Al_{67}N$ films.

also triggers in part the spinodal decomposition at ~800 °C. The identification of such molecular nitrogen "third phase", observed for samples annealed at 900 °C and 1000 °C, was further investigated using second-order synchrotron X-ray techniques and is presented and discussed in detail in the following section.

3.3. Resonant inelastic X-ray scattering and X-ray emission features

RIXS and X-ray emission spectroscopy (XES) are element-sensitive techniques employed to gather information on the occupied density of states. By tuning the excitation energy just above the absorption edge of a certain element, one can obtain the partial density of states (p-DOS) of this element in the VB (normal X-ray emission). In contrast, when the energy of the incident radiation is tuned to resonantly knock out an inner shell electron to an unoccupied excited state of the atom, it is possible to obtain the character of the electronic excitation of that intermediate state using RIXS. Fig. 5a–c shows the RIXS spectra at the N 1s from TiN, h-AlN and a $Ti_{33}Al_{67}N$ film annealed in vacuum at 1000 °C, respectively. Fig. 5a shows that TiN has metallic character, as there is finite DOS at the Fermi level, connecting the VB and the conduction. The observed RIXS spectra correlate well with the original reference on RIXS, where TiN was used as the first testing material [3]. In contrast, Fig. 5b shows the insulating character of h-AlN with a band gap of ~6 eV, which is in good agreement with the recent value reported by Magnuson et al. [31]. Fig. 5c shows a superposition of two components of TiN and AlN, as one can clearly see from the 435 eV-excited spectrum. The lowest part of the $Ti_{1-x}Al_xN$ CB has TiN character which contributes to the metallic character. The SXA peaks > 401.6 eV are clearly of AlN character, since the resonantly excited spectra showed a full-width at half maximum (FWHM) (1.3 eV) close to that of AlN.

However, the resonantly excited $Ti_{1-x}Al_xN$ at 401.2 eV is not exactly the same as the corresponding TiN or AlN spectra, so the mixed film is not a simple mixing of aluminum nitride and titanium nitride. Instead, as described in the previous section, a small amount of molecular nitrogen appears to be formed upon decomposition. Concerning the annealed $Ti_{33}Al_{67}N$ sample, it is observed that the FWHM of the RIXS spectra at 401.6 eV and above is ~1.3 eV, which is similar to that observed in h-AlN RIXS (Fig. 5b), while the FWHM of the RIXS spectra <400.0 eV matches those for TiN RIXS (Fig. 5a). In

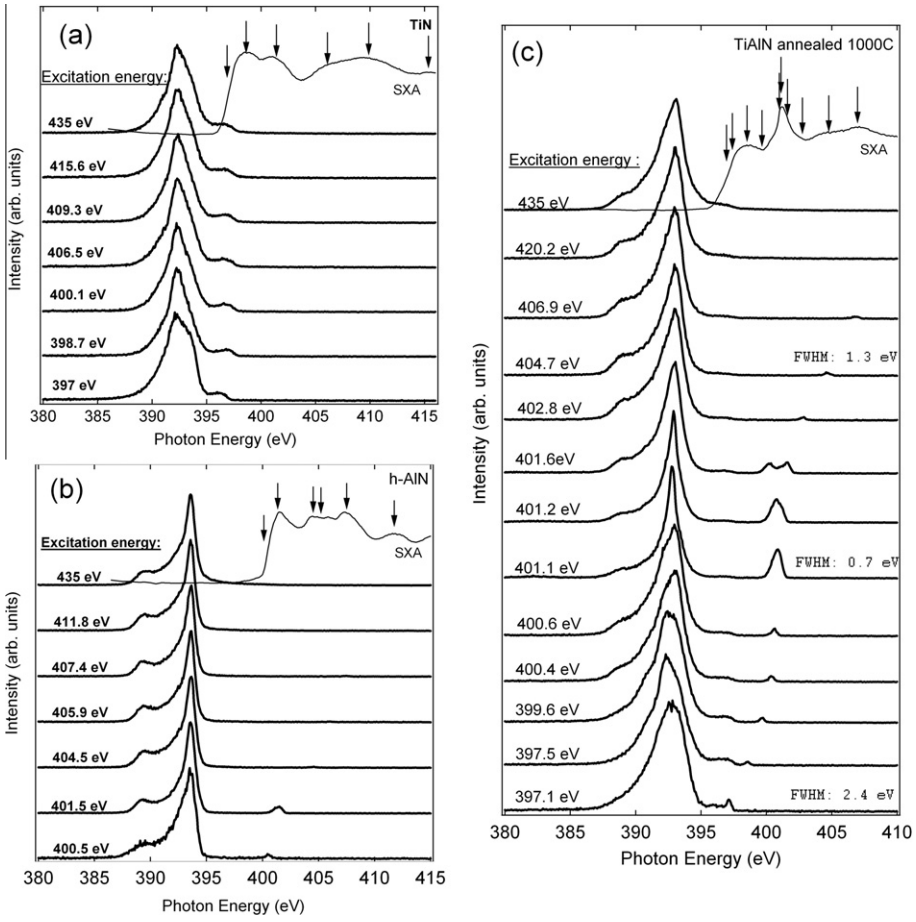

Fig. 5. N *K*-edge RIXS spectra: (a) TiN; (b) h-AlN; (c) $Ti_{33}Al_{67}N$ film annealed in vacuum at 1000 °C. The FWHM is indicated for several RIXS spectra of the sample annealed at 1000 °C.

addition, the lineshape of RIXS spectra in the high energy range (>401.6 eV) shows a small feature ~4 eV lower than the main valence peak, while the RIXS spectra in the low energy range (<400.0 eV) show a small shoulder ~3.5 eV higher than the main VB peak, in good correlation with the h-AlN and TiN RIXS spectra shown as standards. In the middle energy range, there is a resonance at 401 eV, which cannot be correlated to RIXS spectra of either h-AlN or TiN and seems to be associated with the absorption peak for molecular nitrogen. If N is not bound to any other element, but just as a molecule, its states are molecular and, consequently, very localized. In this case, a core hole would decay by a resonant process involving the same electron previously excited. The observation of the resonance would be a proof of the highly localized character of the N states at this peak and, consequently, of their molecular character. The presence of molecular nitrogen by X-ray absorption has been reported during the oxide formation of titanium-based nitride films [32] as well as during high-energy N_2^+ implantation in Ti surfaces [33], with the feature being associated with the replacement or saturation of Ti–N bonds. Moreover, the formation of molecular dinitrogen species has also been reported recently in alumina samples as well as in GaAs, InSb and InAs semiconductors upon low-energy N_2^+ ion bombardment [34,35]. In those cases, it was speculated that the dinitrogen molecules remain trapped in either vacancy or interstitial sites. While it is not possible, at the present stage, to determine the mechanism by which such molecular dinitrogen species form in the composite fine structure of decomposed supersaturated $Ti_{1-x}Al_xN$ films, one can speculate that, during the segregation of the h-AlN phase and owing to the inhomogeneous distribution of Al in the films [6], two nitrogen atoms would coincide locally and associate into a molecule, remaining trapped in the grain boundaries of the formed nanocomposite. In addition, the formation of N_2 could be attributed to the replacement of a small part of the N bonds in c-TiN domains, formed during the decomposition, by the residual oxygen within the films, as has been observed in the oxidation of pure TiN films [33]. Independently of the mechanism by which these dinitrogen species are formed, the molecules remain trapped in the film up to at least 1000 °C and therefore could play a role in the reported high micro-stress levels observed by high resolution transmission electron microscopy and the overall physical properties of decomposed $Ti_{1-x}Al_xN$ films [4,5].

Fig. 6 shows soft X-ray emission spectra at the N *K*-edge of $Ti_{1-x}Al_xN$ films as deposited and annealed at 700, 800 and 1000 °C measured at an excitation energy of 435 eV. Reference spectra of h-AlN (bottom) and TiN (top) are also shown for comparison. Consequently, Fig. 5 shows the occupied N-p partial DOS of the VB in the different samples.

Some differences can be observed between the $Ti_{1-x}Al_xN$ samples, both in the energy position of the top of the band and in the spectral shape. The position of the top of the band can be associated with the band

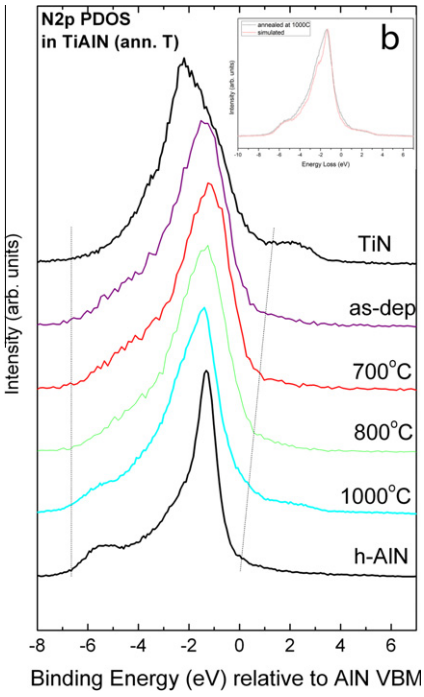

Fig. 6. N *K*-emission spectra (only the valence-band emission is shown). The spectra are plotted relative to the binding energy of the VBM of h-AlN. The dashed lines indicate the motion of the top and bottom of the VB, and are guides to the eye. Inset shows the good fit of the emission spectra for the sample annealed at 1000 °C and that of simulated emission spectra of TiN (35%) and h-AlN (65%).

gap width [36]. The higher the energy of the top of the band, the narrower the band gap becomes. The samples show a trend for the band gap between the as-deposited sample and that at 800 °C to increase upon annealing. The sample annealed at 1000 °C apparently follows the same trend, but the small feature observed near 2 eV, similar to that observed for the TiN reference, indicates that this sample has an apparent lack of band gap similar to TiN. However, one should be very careful assigning a band gap value, since that band gap would correspond only to the formed c-TiN domains, which account only for about one-third of the entire film.

Concerning the spectral shape, there is no apparent change between the as-deposited sample and those annealed at 700 and 800 °C as was the case with N 1s TFY XANES spectra (Fig. 3c). However, the sample annealed at 1000 °C shows clear differences. First, there is a small bump at 2 eV, as mentioned above, which could indicate the precipitation of TiN in this sample. The main peak is slightly shifted to a position close to that of h-AlN, with a shoulder at the lower energy side which coincides with the position of the main peak of TiN. In addition, a clear peak is observed at −5 eV, which correlates with a similar peak present in the h-AlN sample. All these observations suggest that in this sample a phase separation into h-AlN and TiN has occurred. The 1000 °C XES spectrum was compared against a spectrum constructed by superposing 65% h-AlN and 35% TiN spectra (inset in Fig. 6). The

model spectrum fit the observed spectrum quite closely, indicating the overall chemical composition is largely maintained besides the formation of molecular dinitrogen species.

4. Conclusions

This paper has shown the beautiful structural electronic fingerprints of a long discussed and contended decomposition process. The structural features that indicate that h-AlN domains start to form already at 900 °C, and from N *K*-edge it was demonstrated that the decomposed film is not a simple mixture of c-TiN and h-AlN. Despite the difficulty in identifying phase transformations in the material, owing to its complex fine-grained structure, the combination of X-ray absorption, X-ray emission and RIXS spectroscopy proved to be a useful approach in combination with XRD data and simulation from first principles to uncover detailed evidence of spinodal decomposition, phase transformation and molecular nitrogen in the samples. These results should be of use in understanding such structural changes in $Ti_{1-x}Al_xN$ and provide proof from the electronic structure to other experimental tests reported in the literature.

The Ti *K*-edge in titanium aluminum nitride films matched the spectrum of the TiN sample upon annealing at 900 °C; this was a clear evidence that the phase decomposition had taken place. Then, at the same temperature, the formation of h-AlN was evidenced by the Al *K*-edge XANES, while <900 °C the Al *K* XANES peak remained mostly cubic, which is consistent with the two-step decomposition process as well as with X-ray emission data for the N *K*-edge, which also showed the nucleation of the h-AlN phase at temperatures >800 °C. The RIXS technique near the N *K*-edge revealed the nanocomposite formation of the films upon annealing at 1000 °C by comparing the lineshape and FWHM of the RIXS spectra with that of the RIXS features of TiN and h-AlN standards. It was found that the resonantly excited $Ti_{1-x}Al_xN$ at ~401.2 eV did not match the RIXS spectra for TiN or AlN, so it was determined that the mixed film is not a simple mixing of aluminum nitride and titanium nitride and that there is a small amount of molecular nitrogen appearing upon decomposition. The formation of molecular di-nitrogen molecules could be due to the presence of interstitial nitrogen in the as deposited sample together with the structural disorder and irregular distribution of the metal components in supersaturated $Ti_{1-x}Al_xN$. The dinitrogen molecules remain trapped at the grain boundaries of the formed nanocomposite sample up to at least 1000 °C. The decomposition process of the c-$Ti_{1-x}Al_xN$ is further evidenced by the fact that it was possible to obtain a close match between the XES spectra for the sample annealed at 1000 °C and a simulated spectrum composed of a 35% c-TiN and 65% h-AlN composite. Moreover, the data presented have now triggered in-depth theoretical studies, which are currently under way, since for the first time it is possible to correlate the electronic structure as calculated by state-of-the-art computer models to one comprehensive experimental data set. This is of prime importance for the refinement of computer models to handle more complex materials and transformations than is currently possible.

Acknowledgements

This work was partially supported by the Spanish MICINN through projects MAT2007-66719-C03-03, FIS2009-12964-C05-04 and project Consolider Ingenio CSD2008-00023. One of the authors (J.L.E.) thanks the Spanish Ministerio de Educación y Ciencia (MEC) for financial support through the "Ramón y Cajal" Programme. J.A. was supported by the Wenner-Gren Foundations and the SSF program MS2E. The authors also thank Mr. Y.S. Liu (ALS) for beamline assistance and Mr Jim Garrett (McMaster) for performing sample annealing in vacuum. the authors gratefully acknowledge beamtime at the 7.0.1 beamline (ALS, Berkeley), the SGM beamline at (CLS, Saskatoon) and the KMC-2 beamline (BESSY, Berlin). The research performed at the Canadian Light Source is supported by NSERC, NRC, CIHR and the University of Saskatchewan. The synchrotron work at BESSY-II was supported by the EC "Research Infrastructure Action" under the FP6 "Structuring the European Research Area Programme" through the "Integrated Infrastructure Initiative Integrating Activity on Synchrotron and Free Electron Laser Science" (Contract No. R II 3-CT-2004-506008). The Advanced Light Source is supported by the Director, Office of Science, Office of Basic Energy Sciences of the U.S. Department of Energy under Contact No. DE-AC02-05CH11231.

References

[1] Kalss W, Reiter A, Derflinger V, Gey C, Endrino JL. Int J Refract Met Hard Mater 2006;24:399.
[2] Fox-Rabinovich G, Veldhuis SC, Kovalev AI, Wainstein DL, Gershman IS, Korshunov S, et al. J Appl Phys 2007;102:074305.
[3] Rubensson JE, Wassdahl N, Bray G, Rindstedt J, Nyholm R, Cramm S, et al. Phys Rev Lett 1988;60:1759.
[4] Fox-Rabinovich GS, Endrino JL, Beake BD, Aguirre MH, Veldhuis SC, Quinto DT, et al. Surf Coat Technol 2008;202:2985.
[5] Hörling A, Hultman L, Oden M, Sjolen J, Karlsson L. J Vac Sci Technol 2002;20:1815.
[6] Mayrhofer PH, Hörling A, Karlsson L, Sjolen J, Larsson T, Mitterer C, et al. Appl Phys Lett 2003;83:2049.
[7] Fox-Rabinovich GS, Endrino JL, Beake BD, Kovalev AI, Veldhuis SC, Ning L, et al. Surf Coat Technol 2006;201:3524.
[8] Ye M, Berton G, Delplancke JL, Delplancke MP, Segers L, Winand R, et al. Mater Sci Forum 1998;287–288:275.
[9] Endrino JL, Fox-Rabinovich GS, Gey C. Surf Coat Technol. 2006;200:6840.
[10] Alling B, Ruban AV, Karimi A, Peil OE, Simak SI, Hultman L, et al. Phys Rev B 2007;75:045123.
[11] Gago R, Redondo-Cubero A, Endrino JL, Jimenez I, Shevchenko N. J Appl Phys 2009;105:113521.
[12] Tuilier MH, Pac MJ, Girleanu M, Covarel G, Arnold G, Louis P, et al. J Appl Phys 2008;103:083524.
[13] Endrino J, Palacín S, Gutiérrez A, Schäffers F, Krzanowski J. J Mater Sci 2007;42:7607.

[14] Mayrhofer PH, Hultman L, Schneider JM, Staron P, Clemens H. Int J Mater Res 2007;98:1054.
[15] Knutsson A, Johansson MP, Persson POA, Hultman L, Oden M. Appl Phys Lett 2008;93:143110.
[16] Mayrhofer PH, Music D, Schneider JM. Appl Phys Lett 2006;88:071922.
[17] Menzel S, Göbel T, Bartsch K, Wetzig K. Surf Coat Technol 2000;124:190.
[18] Hugosson HW, Jansson U, Johansson B, Eriksson O. Science 2001;293:2434.
[19] Escudeiro Santana A, Karimi A, Derflinger VH, Schütze A. Thin Solid Films 2004;469–470:339.
[20] Kresse G, Furthmüller J. Comput Mater Sci 1996;6:15.
[21] Blochl PE. Phys Rev B 1994;50:17953.
[22] Herman F, Van Dyke JP, Ortenburger IB. Phys Rev Lett 1969;22:807.
[23] Perdew JP, Burke K, Ernzerhof M. Phys Rev Lett 1996;77:3865.
[24] Nordgren J, Bray G, Cramm S, Nyholm R, Rubensson JE, Wassdahl N. In: International conference on synchrotron radiation instrumentation. Tsukuba: AIP; 1989. p. 1690.
[25] Klug HP, Alexander LE. X-Ray diffraction procedures for polycrystalline and amorphous materials. New York: Wiley; 1974.
[26] Mizoguchi T, Tanaka I, Yoshioka S, Kunisu M, Yamamoto T, Ching WY. Phys Rev B 2004;70:045103.
[27] Ersen O, Tuilier MH, Thomas O, Gergaud P, Lagarde P. Appl Phys Lett 2003;82:3659.
[28] Sennour M, Esnouf C. Acta Mater 2003;51:943.
[29] Mazor A, Srolovitz DJ, Hagan PS, Bukiet BG. Phys Rev Lett 1988;60:424.
[30] Lawniczak-Jablonska K, Suski T, Liliental-Weber Z, Gullikson EM, Underwood JH, Perera RCC, et al. Appl Phys Lett 1997;70:2711.
[31] Magnuson M, Mattesini M, Hoglund C, Birch J, Hultman L. Phys Rev B 2009;80:155105.
[32] Esaka F, Furuya K, Shimada H, Imamura M, Matsubayashi N, Kikuchi T, et al. Surf Interface Anal 1999;27:1098.
[33] Soriano L, Abbate M, Fuggle JC, Jiménez C, Sanz JM, Galán L, et al. Surf Sci 1993;281:120.
[34] Hecht JD, Frost F, Hirsch D, Neumann H, Schindler A, Preobrajenski AB, et al. J Appl Phys 2001;90:6066.
[35] Holgado JP, Yubero F, Cordón A, Gracia F, González-Elipe AR, Avila J. Solid State Commun 2003;128:235.
[36] Duda LC, Stagarescu CB, Downes J, Smith KE, Korakakis D, Moustakas TD, et al. Phys Rev B 1998;58:1928.